Electrochimica Acta 77 (2012) 324–329

Contents lists available at SciVerse ScienceDirect

Electrochimica Acta

journal homepage: www.elsevier.com/locate/electacta

Synthesis and characterization of non-precious metal binary catalyst for oxygen reduction reaction in proton exchange membrane fuel cells

Hui-Juan Zhang[a,b], Xianxia Yuan[b,*], Liangliang Sun[c], Junhe Yang[a], Zi-Feng Ma[b,*], Zongping Shao[c]

[a] School of Materials Science and Engineering, University of Shanghai for Science and Technology, Shanghai 200093, China
[b] Department of Chemical Engineering, Shanghai Jiao Tong University, Shanghai 200240, China
[c] School of Chemistry and Chemical Engineering, Nanjing University of Technology, Nanjing 210009, China

ARTICLE INFO

Article history:
Received 27 April 2012
Received in revised form 5 June 2012
Accepted 5 June 2012
Available online 15 June 2012

Keywords:
Non-precious metal catalyst
FeCoTETA/C
Oxygen reduction reaction
Proton exchange membrane fuel cells (PEMFCs)

ABSTRACT

A promising non-precious metal FeCoTETA/C catalyst has been easily synthesized, by chelating Fe and Co with triethylenetetramine (TETA) in ethanol followed by pyrolyzing in an Ar atmosphere, as electrocatalyst for oxygen reduction reaction (ORR) in proton exchange membrane fuel cells (PEMFCs). The catalyst has been characterized with various physicochemical techniques as well as electrochemical analysis and single cell performance measurement. The results showed that nano-intermetallic FeCo particles and several types of N and O species are present on carbon matrix. The catalyst delivers better electrocatalytic activity toward ORR compared with CoTETA/C catalyst, the $\%H_2O_2$ is about 10% with an electron-transfer number of around 3.8. The PEMFC with this catalyst in cathode reaches a maximum power density of 256 mW cm^{-2} and has a current density of 514 mA cm^{-2} at 500 mV.

1. Introduction

Renewable energy sources attract growing attention to fulfill the energy requirements in the future while simultaneously reduce environment pollution. Cheap efficient catalysts with abundant raw materials for oxygen reduction reaction (ORR) are strongly needed in order for large scale commercialization of proton exchange membrane fuel cells (PEMFCs). Until now, Pt-based catalysts have been approved to be the best ones for the ORR in PEMFCs. However, Pt is an expensive metal of limited supply. Therefore, partial or complete replacement of Pt with non-precious metal in ORR catalysts is of worldwide interest and much progress has been made so far [1–3]. Some Pt-free catalysts, such as Fe/N/C [4], carbonized hemoglobin [5], CoTMPP/C [6], Co-PPy/C [7–9], and CoTETA/C [10], have been successfully developed in recent years and have shown promising catalytic performance toward ORR in PEMFCs.

The activity and selectivity of a monometallic catalyst can be greatly improved if a second metal is introduced to form a bimetallic catalyst. Typical examples are PtPd [11] and $Pt_3Ni(1\,1\,1)$ [12] bimetallic catalysts. The introduction of Pd or Ni has significantly enhanced the catalytic activity compared with a Pt monometallic catalyst [11,12]. Metal alloys supported on carbon powder are commonly employed as heterogeneous catalysts. For example, Pt-based alloy/carbon nanocomposites, such as PtCo/C, PtNi/C and PtCr/C [13,14], are receiving great attention as cathode catalysts for low temperature fuel cells. Heat-treated binary-metal tetraphenylporphyrin (TMTPP, TM = V/Fe, Co/Fe, Ni/Fe, and Cu/Fe) have shown excellent activity toward ORR [15]. These catalysts were usually prepared from mixed-metal carbonyl cluster complexes or mixed metal macrocycle compounds, which caused high cost and difficult preparation.

A discovery of improved catalysts with low-cost, such as cheap and abundant raw materials, is the most favorite for wide use in PEMFCs. Recently, we have employed triethylenetetramine (TETA), a simple and cheap ligand, to prepare non-precious metal Co-based catalyst for the ORR [10–12]. Furthermore, we have found that the 3d transitional metals play an important role on the catalytic performance of metal-TETA/C catalysts [16]. In this paper, we study the catalytic activity of the binary catalyst when Co is partly replaced by Fe, in order to further improve the catalytic performance of CoTETA/C catalyst and reduce the cost. The structure and morphology of the obtained FeCoTETA/C catalyst have been characterized by X-ray diffraction (XRD), transmission electron microscopy (TEM) combined with energy dispersive X-ray spectroscopy (EDX), and X-ray photoelectron spectroscopy (XPS). Electrochemical performance of the catalyst toward ORR has been demonstrated by cyclic voltammogram (CV), rotating disk electrode (RDE), and rotating ring-disk electrode (RRDE) measurements in oxygen-saturated acidic solution, as well as in a single PEMFC test.

* Corresponding authors. Tel.: +86 21 54742827; fax: +86 21 54741297.
E-mail addresses: yuanxx@sjtu.edu.cn, yuanxx519@yahoo.com.cn (X. Yuan), zfma@sjtu.edu.cn (Z.-F. Ma).

0013-4686/$ – see front matter © 2012 Elsevier Ltd. All rights reserved.
http://dx.doi.org/10.1016/j.electacta.2012.06.011

2. Experimental

2.1. Catalysts preparation

A facile synthetic method was adopted as described elsewhere with some modification [10–12,16]. Briefly, 0.202 g cobalt chloride and 0.242 g iron chloride were dissolved in 50 ml ethanol. Next, 1 ml triethylenetetramine ($H_2NCH_2CH_2NHCH_2CH_2NHCH_2CH_2NH_2$, TETA) was added into the obtained solution followed by 1 g BP 2000. The resulted solution was stirred for 1 h and then dried by rotary evaporator under vacuum. The obtained powder was heat-treated at 800 °C for 90 min in an Ar atmosphere with the temperature raising rate of 5 °C min^{-1}. The total nominal loading of Co and Fe with respect to carbon was kept at 10 wt%. A CoTETA/C catalyst was also prepared with the same procedure for comparison, the amount of used cobalt chloride is 0.404 g to keep the same nominal loading of metal (10 wt%) with respect to carbon in both the FeCoTETA/C catalyst and the CoTETA/C catalyst.

2.2. Physical characterization

The XRD was performed on an automated Rigaku diffractometer equipped with a Cu Kα radiation at a tube current of 30 mA and a tube potential of 40 kV. Data acquisition was recorded in the 2θ range from 20° to 80° at a scan rate of 6° min^{-1}. The PDF (powder diffraction file database) from the ICDD (International Centre for Diffraction Data) was used as reference to interpret peak assignments in the XRD spectra.

TEM and EDX measurements were performed at a JEOL JEM-2010 operating at 200 keV. The catalyst was ultrasonically stirred in ethanol absolute for 5 min. A drop of the solution was deposited onto a carbon-coated copper grid and left in air to dry.

Electronic structures of C, N and O on the catalyst surface were evaluated by XPS, which was carried out on a RBD upgraded PHI-5000C ESCA system (Perkin Elmer) with Mg Kα radiation ($h\nu$ = 1253.6 eV). The sample was directly pressed to a self-supported disk (10 mm × 10 mm) and mounted on a sample holder then transferred into the analyzer chamber. The whole spectra and the narrow spectra of several elements with high resolution were both recorded by using RBD 147 interface (RBD Enterprises, USA) through the AugerScan 3.21 software. Binding energies were calibrated by using the containment carbon (C1s = 284.6 eV). The data analysis was carried out by using the RBD AugerScan 3.21 software provided by RBD Enterprises or XPSPeak4.1 provided by Raymund W.M. Kwok (The Chinese University of Hongkong, China).

2.3. Electrochemical characterization

Electrochemical characterizations were performed in a single-compartment, three-electrode cell filled with 0.5 M H_2SO_4 solution at room temperature. A rotating disk electrode with a glassy carbon disk (4.0 mm in diameter) was used as the working electrode. A Pt wire and a saturated calomel electrode were used as the counter and reference electrode, respectively. All potentials in this paper are referred to the normal hydrogen electrode (NHE). An ink-type electrode was prepared as follows: 5 mg finely ground catalyst powder, 0.5 ml doubly distilled water and 50 μl 5 wt% Nafion solution were blended in an ultrasonic bath, then 10 μl of this ink was deposited onto the surface of a glassy carbon disk and air-dried for use.

Before electrochemical measurements, the electrolyte solution was purged with pure oxygen for 15 min. Then, cyclic voltammograms (CVs) were repeated at a potential sweep rate of 50 mV s^{-1} in a range from 1.04 V to 0.04 V to remove any impurities and reach a steady performance. A CV curve was then recorded at the potential scan rate of 5 mV s^{-1}. For rotating disk electrode (RDE) study, the current–potential polarization curves were obtained at various electrode rotation speeds from 100 rpm to 900 rpm. For rotating ring-disk electrode (RRDE) study, a Pt disk-Pt ring electrode (5 mm in diameter for the Pt-disk) was employed, and 10 μl of the catalyst ink prepared with the same procedure was dropped onto the disk only, and the ring potential was kept at 1.2 V.

All electrochemical measurements were operated using a 750A bipotentiostat (CHI instrument, USA) along with a 636 RRDE system (Pine instrument, USA) at room temperature.

2.4. Single cell test

Single cell performance based on FeCoTETA/C as well as Pt/C as cathode catalyst, respectively, was examined under actual H_2–O_2 PEMFC condition. The surface area used for the fuel cell test was 2.5 cm × 2.5 cm. The preparation of MEA follows the procedure described in literature [17]. A non-precious metal cathode electrode was formed by ultrasonically blending 20 mg FeCoTETA/C catalyst powder with 0.2 g 5 wt% Nafion® solution in ethanol for 1 h and depositing the ink on the gas diffusion layer. A Pt/C cathode electrode was prepared by ultrasonically blending 20 mg 20 wt% Pt/C catalyst powder (Johnson Matthey) with 0.2 g 5 wt% Nafion® solution in ethanol for 1 h and depositing the ink on the gas diffusion layer. The anode with Pt loading of 1 mg cm^{-2} was formed using a catalyst paste prepared by dispersing 10 mg 20 wt% Pt/C into a solution containing ethanol absolute and 0.1 g 5 wt% Nafion® solution. Both hydrogen and oxygen were non-humidified and passed into the apparatus at 200 ml min^{-1}. The current–potential relationships were recorded at 50 °C when the fuel cell performance was steady.

3. Results and discussion

3.1. XRD analysis

Fig. 1 displays the XRD patterns of (a) the FeCoTETA/C catalyst and (b) the CoTETA/C catalyst. The standard diffraction peaks of FeCo (PDF 65-4131) and α-Co (PDF 89-4307) are also shown for comparison. Several characteristics could be found in Fig. 1: (1) for each catalyst, there is a large broad diffraction peak around 24.5° which can be ascribed to the characteristic peak of the C(0 0 2); (2) for the FeCoTETA/C catalyst, there are two diffraction peaks at 45° and 65°, which can be ascribed to the characteristic peaks of FeCo(1 1 0) and FeCo(2 0 0), respectively. This indicates that face-centered cubic (*fcc*) crystalline FeCo particles appear on carbon matrix in the FeCoTETA/C catalyst; and (3) the CoTETA/C catalyst

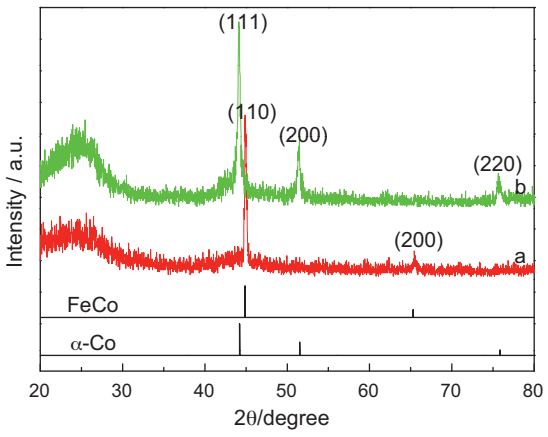

Fig. 1. XRD patterns of (a) the FeCoTETA/C catalyst and (b) the CoTETA/C catalyst. Standard characteristic diffraction peaks of FeCo (PDF 65-4131) and α-Co (PDF 89-4307) are also shown for comparison. Each spectrum is arbitrarily shifted for easier comparison.

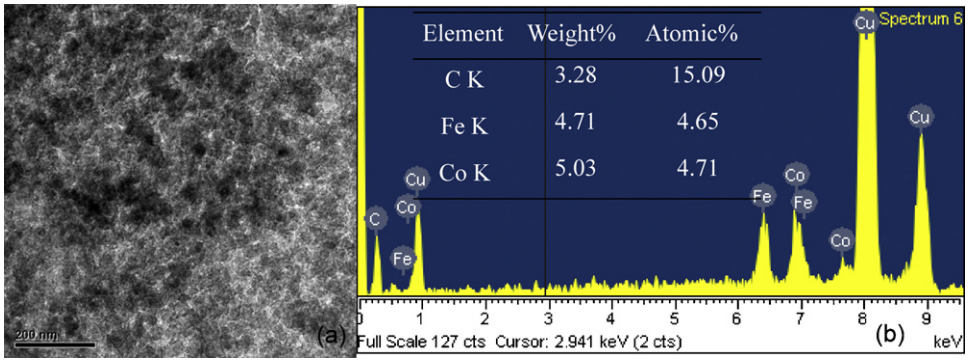

Fig. 2. (a) TEM image and (b) EDX analysis of the FeCoTETA/C catalyst.

clearly shows the presence of metallic α-Co with three characteristic peaks at 44.2°, 51.5° and 75.8°, which are signed to Co (1 1 1), Co(2 0 0) and Co(2 2 0) plane, respectively.

3.2. TEM and EDX analysis

A visual confirmation of the presence of FeCo particles is given in Fig. 2(a), where a TEM micrograph of the FeCoTETA/C catalyst is shown with a multiple of 200 nm. The gray area is attributed to the basic macrostructure of amorphous carbon framework and the small black spots are due to the large thickness of the intermetallic FeCo particles. It can be seen that the distributions of the FeCo particles are not quite uniform, which may be caused by the high temperature treatment and the easy transfer of Fe and Co during pyrolysis. This phenomenon is consistent with the XRD analysis in Fig. 1.

EDX analysis of the FeCoTETA/C catalyst (Fig. 2(b)) reveals that the at% of Fe and Co in this catalyst is 4.65 and 4.71, respectively. It confirms the actual atomic ratio of Fe:Co = 1:1 in the obtained FeCoTETA/C catalyst, agreeing well with the designed atomic ratio. Cu peak in the EDX spectrum is from the substrate used during the TEM and EDX measurements.

3.3. XPS analysis

XPS survey spectrum of the FeCoTETA/C catalyst is given in Fig. 3. It clearly shows a predominant C 1s peak at 285 eV, a weak O 1s peak at 532 eV and a much weaker N 1s peak at 400 eV. These weak peaks of O 1s and N 1s in the XPS spectra presumably arise from the physically adsorbed oxygen-containing functional groups and nitrogen-containing species on the carbon surface [18].

Regarding the C 1s region as shown in Fig. 4(a), the peak shifts to a higher binding energy of 284.8 eV, as compared to the peak of 284.5 eV that has been observed for a

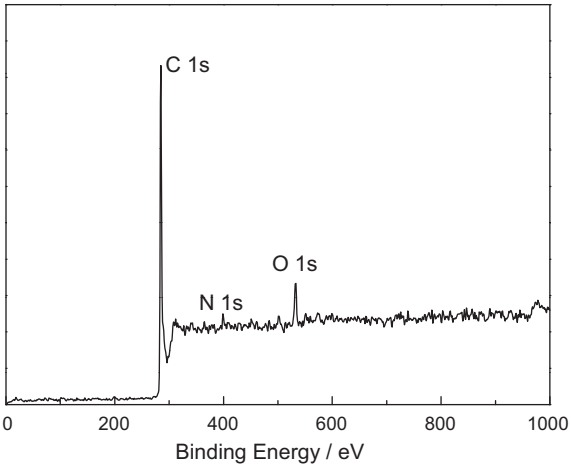

Fig. 3. The whole XPS survey for the FeCoTETA/C catalyst.

number of carbon supports such as Norit SX Ultra [19] and Vulcan SC-72R [20]. This could be attributed to the adulteration of nitrogen atoms and oxygen species on the carbon support. The C 1s spectra can be decomposed into three peak components at 284.8 eV, 285.4 eV and 288.3 eV, which could be assigned to the carbon component in C—C, C—O and O=C—O, respectively.

Several different N coordinations with close binding energies have been reported in the literatures [21]: (1) pyridinic N with its peak at 398.3–399.5 eV; (2) pyrrolic N with its peak at 399.9–400.7 eV; and (3) graphitic N with its peak at 401–403 eV. The XPS of N 1s in the FeCoTETA/C catalyst as displayed in Fig. 4(b) can be deciphered into pyridinic N, pyrrolic N and graphitic N with the contributions of 26%, 36% and 38%, respectively. This indicates the incorporation of nitrogen within the graphene sheets.

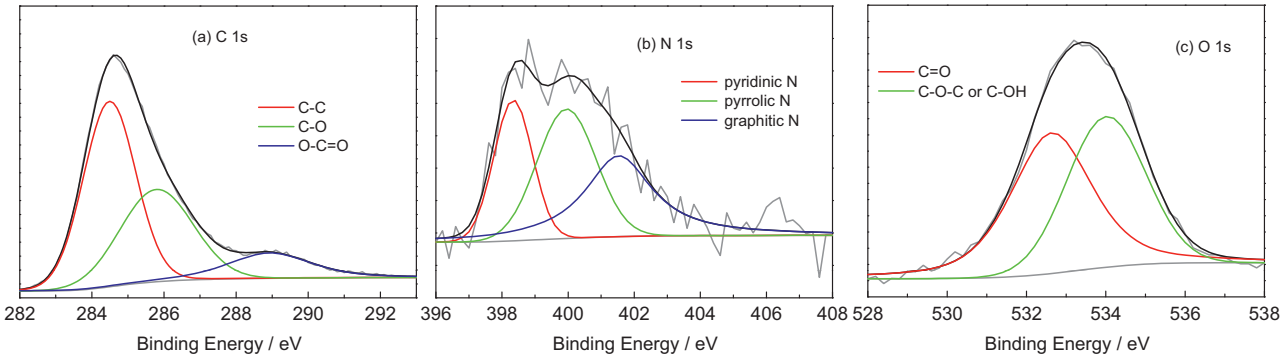

Fig. 4. High-resolution XPS of (a) C 1s, (b) N 1s and (c) O 1s for the FeCoTETA/C catalyst.

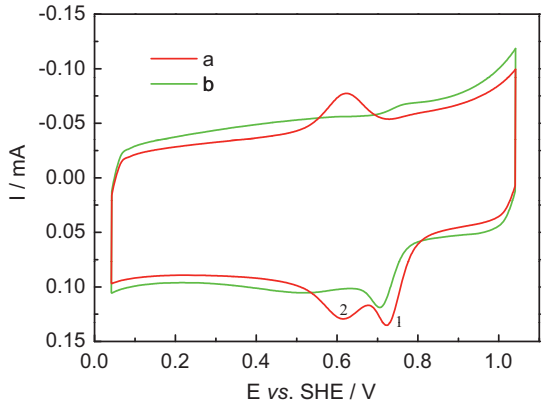

Fig. 5. Cycle voltammograms of (a) the FeCoTETA/C catalyst and (b) the CoTETA/C catalyst in oxygen-saturated 0.5 M H_2SO_4 solution at a scan rate of 5 mV s^{-1}.

According to Sidik et al.'s study on cluster models of graphite sheets containing substitutional N toward oxygen reduction reaction in acidic media [22], pyridinic N has one lone pair of electrons in addition to the one electron donated to the conjugated π bond system, imparting a Lewis basicity to the carbon, and it is capable of facilitating the reductive adsorption reaction of O_2 without the irreversible formation of oxygen functionalities, due to an increased electron-donor property of carbon.

Similar to the investigation on Fe-based cathode catalyst by Jaouen et al.'s [23], the XPS O 1s narrow-scan spectra presented in Fig. 4(c) can be decomposed into two components: O_A at a binding energy of 532.6 eV assigned to C═O (aldehydes, ketones and lactones) and O_B at 534 eV assigned to the C—OH and/or C—O—C groups. Moreover, the fact that comparable contents of O_A and O_B implies similar amount of functional groups of C═O and C—OH and/or C—O—C in the FeCoTETA/C bimetallic catalyst.

3.4. Electrochemical characterization

Fig. 5 presents the cyclic voltammograms of the FeCoTETA/C catalyst performed in oxygen-saturated 0.5 M H_2SO_4 solution, which provides information on the electrochemical oxygen reduction properties of the catalysts. For comparison, the CV curve measured on the CoTETA/C catalyst is also shown in Fig. 5. As we can see, there are two obvious consecutive reduction peaks in the negative scan and one oxidation peak in the reverse scan for the bimetallic FeCoTETA/C catalyst, while only one reduction peak could be observed for the CoTETA/C catalyst. For the two reduction peaks of FeCoTETA/C catalyst, peak 1 at 724 mV represents the electrochemical reduction of oxygen, peak 2 at 618 mV along with the oxidation peak at about 620 mV reveals a pair of well-developed quasi "reversible" redox processes between Fe(II) and Fe(III) species [24–27]. Comparison of the CV curves of FeCoTETA/C and CoTETA/C reveals an obvious higher ORR peak potential of the former, indicating better catalytic performance toward oxygen reduction in acidic media. Therefore, it could be figured out that catalytic activity of CoTETA/C for ORR could be improved by partially replacing Co with Fe.

Fig. 6(a) shows the typical polarization curves of the FeCoTETA/C catalyst on rotating disk electrode performed in oxygen-saturated 0.5 M H_2SO_4 solution using a potential scan rate of 5 mV s^{-1} and with the rotation speed from 100 rpm to 900 rpm. Independent non-zero current values appear from 740 mV to 1000 mV. A well-defined diffusion limiting current plateau is reached below 600 mV and mass transport contributions are not very obvious at these potentials. But for the potential range between 600 mV and 740 mV, there are no well-defined diffusion limiting current plateaus and mass transport contributions become significant. The reason for this phenomenon can be that the mass transport is not simple because of the presence of a rather thick film on the disk and because of diffusion processes in that phase, and perhaps also due to the distribution of the active sites. When the distribution of the electrocatalytic active sites is uniform and the reaction is slow, the current–potential polarization plateau is not quite inclined [28]. Another more possible explanation for this phenomenon is that the electrocatalytic active sites are distributed on the carbon surfaces but not in the pores of carbon. In this situation, the ORR processes enough and when the potential changes, the current changes sharp.

Using data from the RDE measurements, Koutecky–Levich plots are determined with the following equations [28,29]:

$$I^{-1} = I_k^{-1} + I_d^{-1} = I_k^{-1} + (B\omega^{1/2})^{-1} \quad (1)$$

$$B = 0.62nFSC_0D_0^{2/3}\nu^{-1/6} \quad (2)$$

where B is the Levich slope, ω the rotation rate of the working electrode, n the number of electrons transferred per oxygen molecule in the overall reaction, F the Faraday constant, S the electrode surface area (0.1256 cm^2), C_0 the concentration of oxygen dissolved (1.18×10^{-6} mol cm^{-3}), D_0 the diffusion coefficient of oxygen in the solution (1.9×10^{-5} cm^2 s^{-1}), ν the kinematic viscosity of the sulfuric acid (0.00987 cm^2 s^{-1}) [28,29].

A series of Koutecky–Levich plots at a broad potential range from 500 mV to 100 mV are illustrated in Fig. 6(b). At all the rotating rates, a series of essentially parallel straight lines are illustrated, which indicates that the reaction order for the oxygen reduction at the FeCoTETA/C catalyst is unity and follows the first-order kinetics [11]. Parallelism of the straight lines also indicates that the number of transferred-electron per oxygen molecule and active surface area for the reaction does not change significantly within the potential range studied. The non-zero intercept of I^{-1} vs. $\omega^{-1/2}$ plots at

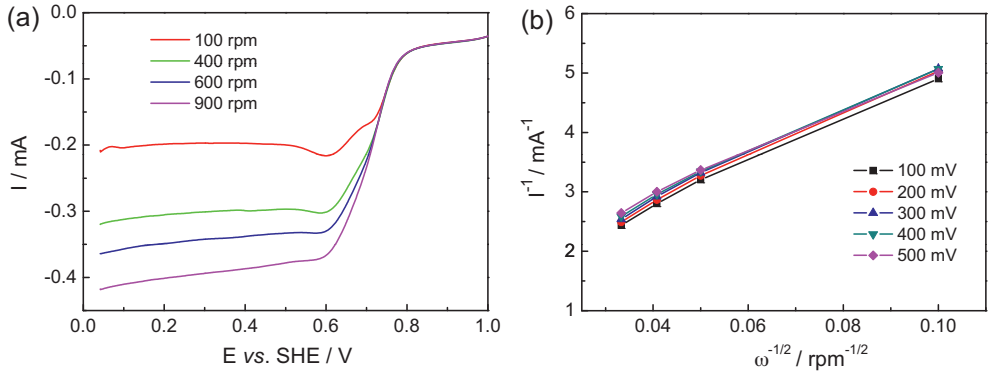

Fig. 6. (a) Current–potential polarization curves and (b) a series of Koutecky–Levich plots of the FeCoTETA/C catalyst in oxygen-saturated 0.5 M H_2SO_4 solution.

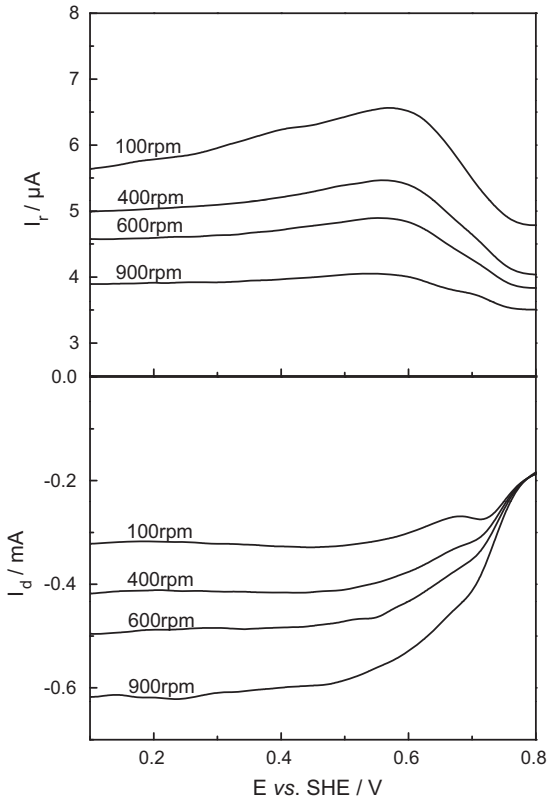

Fig. 7. The disk electrode current I_d and the ring electrode current I_r for the FeCoTETA/C catalyst.

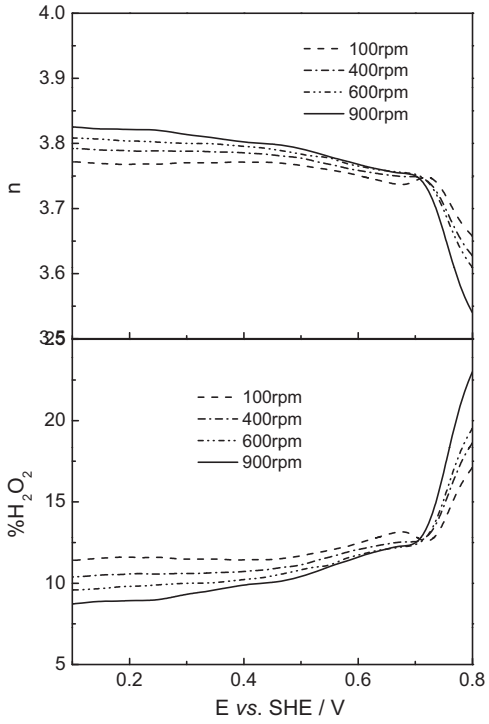

Fig. 8. The $\%H_2O_2$ and the number of electrons transferred n for the FeCoTETA/C catalyst.

the lower electrode potentials ($0.1\,V < E < 0.6\,V$) demonstrates that the effect of the oxygen diffusion in the Nafion layer and the distribution of active sites, as explained above, make it impossible to establish a complete diffusion control [28,29]. This is in agreement with the current–potential polarization curves given in Fig. 6(a), which do not show a well-defined plateau region only for the diffusion-limited processes.

The amount of H_2O_2 produced during oxygen reduction can generally be calculated from the RRDE data using the following equation [30]:

$$\%H_2O_2 = \frac{200(I_r/N)}{I_d + (I_r/N)} \quad (3)$$

where I_d, I_r and N mean the disk current, the ring current and the collection efficiency, respectively. Here, the value of N is taken as 0.39. Fig. 7 presents the I_d and I_r measured at electrode rotating rates from 100 rpm to 900 rpm for the FeCoTETA/C catalyst. It is clear that along the oxygen reduction process the I_d and the I_r change with the potentials. According to Eq. (3), the generated $\%H_2O_2$ is about 10% and the n is around 3.8 as shown in Fig. 8. This value of electron-transfer number is larger than that of 3.6 previously reported for CoTETA/C catalyst [10]. Therefore, it could be suggested that the ORR processes via both the two-electron transfer reduction to generate the H_2O_2 and the four-electron transfer reduction to generate H_2O, but the latter that is the four-electron transfer reaction to water (i.e. $O_2 + 4H^+ + 4e \rightarrow 2H_2O$) is the main process.

3.5. Single cell performance

Single cell performance of a H_2–O_2 PEMFC based on the FeCoTETA/C cathode catalyst is presented in Fig. 9. The cell performance with commercial 20 wt% Pt/C as cathode catalyst is also measured under the same conditions and shown in Fig. 9 for comparison. A current density of 804 mA cm^{-2} at 500 mV and a maximum power density of 559 mW cm^{-2} at 50 °C are obtained for the fuel cell with commercial Pt/C as cathode catalyst, and a current density of 514 mA cm^{-2} at 500 mV and a maximum power density of 256 mW cm^{-2} at 50 °C with non-humidified reaction gases are obtained for the PEMFC with FeCoTETA/C as the cathode catalyst. It is exciting that the performance of the PEMFC with FeCoTETA/C is much higher than those recently reported for non-precious metal catalysts-based PEMFCs, such as Fe-based catalyst (300 mA cm^{-2} at 500 mV, 80 °C) [8,31], Co-PPy-C (200 mA cm^{-2} at 500 mV and a maximum power density of 140 mW cm^{-2} at 80 °C with humidified gases) [8], and CoTETA/C (114 mA cm^{-2} at 500 mV and a maximum power density 162 mW cm^{-2} at 25 °C with non-humidified reaction gases) [10]. In addition, the cell performance is comparable with that using precious metal-based cathode catalysts, such as Pd–Co–Au alloy (180 mA cm^{-2} at 500 mV, 60 °C, 1.5 atm

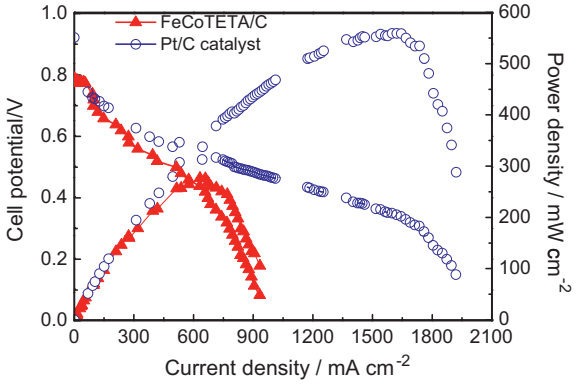

Fig. 9. Single cell performance of a H_2–O_2 PEMFC based on the FeCoTETA/C cathode catalyst. Cell temperature is at 50 °C. Hydrogen and oxygen are non-humidified and pass into the cell apparatus both at 200 ml min^{-1}.

oxygen back pressure) and Pd–Ti alloy (100 mA cm^{-2} at 500 mV, 60 °C) [8,32]. Furthermore, a preliminary comparison between the fuel cell performance with FeCoTETA/C and Pt/C as cathode catalysts, respectively, suggests the potential application of FeCoTETA/C catalyst in PEMFCs, although its performance is still much inferior to Pt/C-based catalysts.

4. Conclusions

In summary, we report a promising non-precious metal FeCoTETA/C catalyst for ORR, which was synthesized from pyrolyzing a carbon-supported iron and cobalt triethylenetetramine binary metal chelate at high temperature in an Ar atmosphere. Results obtained from XRD show that nano-intermetallic FeCo are present in the form of face-centered cubic (*fcc*) structure on carbon matrix. XPS indicates that there are several types of N and O species on the carbon surface. Electrochemical results show that the catalyst displays better ORR catalytic activity as compared to CoTETA/C. The $\%H_2O_2$ and the electron-transfer number during the ORR catalyzed by FeCoTETA/C are calculated to be about 10% and 3.8 with RRDE in an oxygen-saturated H_2SO_4 solution. For an actual H_2–O_2 PEMFC based on this cathode catalyst, the maximum output power density reaches 256 mW cm^{-2} and the current density reaches 514 mA cm^{-2} at 500 mV.

Acknowledgments

The authors are grateful for the financial support of this work by the 973 Program of China (2007CB209700), the National Science Foundation of China (20776085 and 21176155), the STCSM of China (10JC1406900, 09XD1402400, 09520500900) and China Postdoctoral Science Foundation (20100480593).

References

[1] C.W.B. Bezerra, L. Zhang, K. Lee, H. Liu, A.L.B. Marques, E.P. Marques, H. Wang, J. Zhang, Electrochimica Acta 53 (2008) 4973.
[2] B. Wang, Journal of Power Sources 152 (2005) 1.
[3] L. Zhang, J. Zhang, D.P. Wilkinson, H.J. Wang, Journal of Power Sources 156 (2006) 171.
[4] M. Lefèvre, E. Proietti, F. Jaouen, J.P. Dodelet, Science 324 (2009) 71.
[5] J. Maruyama, I. Abe, Chemistry of Materials 18 (2006) 1303.
[6] X.Y. Xie, Z.F. Ma, X. Wu, Q.Z. Ren, X. Yuan, Q.Z. Jiang, L. Hu, Electrochimica Acta 52 (2007) 2091.
[7] X. Yuan, X. Zeng, H.J. Zhang, Z.F. Ma, C.Y. Wang, Journal of the American Chemical Society 132 (2010) 1754.
[8] R. Bashyam, P. Zelenay, Nature 443 (2006) 63.
[9] M. Yuasa, A. Yamaguchi, H. Itsuki, K. Tanaka, M. Yamamoto, K. Oyaizu, Chemistry of Materials 17 (2005) 4278.
[10] H.J. Zhang, X.X. Yuan, W. Wen, D.Y. Zhang, L.L. Sun, Q.Z. Jiang, Z.F. Ma, Electrochemistry Communications 11 (2009) 206.
[11] B. Lim, M. Jiang, P.H.C. Camargo, E.C. Cho, J. Tao, X. Lu, Y. Zhu, Y. Xia, Science 324 (2009) 1302.
[12] V.R. Stamenkovic, B. Fowler, B.S. Mun, G. Wang, P.N. Ross, C.A. Lucas, N.M. Markovic, Science 315 (2007) 493.
[13] A.U. Nilekar, Y. Xu, J. Zhang, M.B. Vulkmirovic, K. Sasaki, R.R. Adzic, M. Mavrikakis, Topics in Catalysis 46 (2007) 276.
[14] S. Chen, P.J. Ferreira, W. Sheng, N. Yabuuchi, L.F. Allard, Y. Shao-Horn, Journal of the American Chemical Society 130 (2008) 13818.
[15] D. Chu, R. Jiang, Solid State Ionics 148 (2002) 591.
[16] H.J. Zhang, Q.Z. Jiang, L.L. Sun, X.X. Yuan, Z.P. Shao, Z.F. Ma, International Journal of Hydrogen Energy 35 (2010) 8295.
[17] L.L. Sun, R. Ran, G. Wang, Z.P. Shao, Solid State Ionics 179 (2008) 960.
[18] K.P. Gong, F. Du, Z.H. Xia, M. Durstock, L.M. Dai, Science 323 (2009) 760.
[19] P. Gouérec, M. Savy, J. Riga, Electrochimica Acta 43 (1998) 743.
[20] G. Faubert, R. Côté, D. Guay, J.P. Dodelet, G. Dénès, C. Poleunis, Electrochimica Acta 43 (1998) 1969.
[21] J. Casanovas, J.M. Ricart, J. Rubio, F. Illas, J.M. Jiménez-Mateos, Journal of the American Chemical Society 118 (1996) 8071.
[22] R.A. Sidik, A.B. Anderson, N.P. Subramanian, S.P. Kumaraguru, B.N. Popov, Journal of Physical Chemistry B 110 (2006) 1787.
[23] F. Jaouen, S. Marcotte, J.P. Dodelet, G. Lindbergh, Journal of Physical Chemistry B 107 (2003) 1376.
[24] A. Velázquez-Palenzuela, L. Zhang, L. Wang, P.L. Cabot, E. Brillas, K. Tsay, J. Zhang, Journal of Physical Chemistry C 115 (2011) 12929.
[25] G. Wu, K.L. More, C.M. Johnston, P. Zelenay, Science 332 (2011) 443.
[26] E. Laviron, Journal of Electroanalytical Chemistry 52 (1974) 395.
[27] K. Kinoshita, J.A.S. Bett, Carbon 11 (1973) 403.
[28] S.Lj. Gojković, S. Gupta, R.F. Savinell, Journal of Electroanalytical Chemistry 462 (1999) 63.
[29] S.Y. Ye, A.K. Vijh, International Journal of Hydrogen Energy 30 (2005) 1011.
[30] V. Nallathambi, J.W. Lee, S.P. Kumaraguru, G. Wu, B.N. Popov, Journal of Power Sources 183 (2008) 34.
[31] C. Medard, M. Lefevre, J.P. Dodelet, F. Jaouen, G. Lindbergh, Electrochimica Acta 51 (2006) 3202.
[32] J.L. Fernandez, V. Raghuveer, A. Manthiram, A.J. Bard, Journal of the American Chemical Society 127 (2005) 13100.